Desalination and Water Treatment
www.deswater.com

doi: 10.5004/dwt.2023.29917

308 (2023) 51–67
October

A full factorial design-based desirability function approach to investigate the transport of Ni^{2+}, Co^{2+}, Cr^{3+} and Zn^{2+} through polymer inclusion membranes

Abdelhamid Cherfi[a,*], Zoulikha Maache-Rezzoug[b], Sid-Ahmed Rezzoug[b]

[a]*Department of Chemistry, Faculty of Sciences, M'hamed Bougara University, 35000 – Boumerdes, Algeria, Tel./Fax: + 21324814376; email: a.cherfi@univ-boumerdes.dz*
[b]*Laboratoire des Sciences de l'Ingénieur pour l'Environnement, LaSIE, UMR CNRS 7356, Université de La Rochelle, Avenue Michel Crépeau, 17042 La Rochelle, France, emails: zoulikha.rezzoug@univ-lr.fr (Z. Maache-Rezzoug), sarezzou@univ-lr.fr (S.-A. Rezzoug)*

Received 22 April 2023; Accepted 25 August 2023

ABSTRACT

In the present study, the full factorial design methodology was used to investigate and optimize the operating conditions of a membrane process involving polymer inclusion membranes (PIMs), for the competitive removal of Ni^{2+}, Co^{2+}, Cr^{3+} and Zn^{2+} from aqueous solutions. The effects of three parameters: initial concentration of metals (X_1), extractant content (X_2) and membrane thickness (X_3) were investigated on the matter fluxes crossing the PIMs (J_i), the amount of metal ions fixed within them (τ_f), and transferred through them (τ_t). The study revealed that: (1) the selectivity order of metal ions crossing the synthesized PIMs is: Zn > Ni > Cr > Co, (2) the order of significance of the effects is: $X_1 > X_2 > X_3$, (3) X_1 and X_2 have positive effect on J, τ_f and τ_t while X_3 has a negative effect on J and τ_t, and (4) the estimated models for the responses fit the experimental data adequately (determination coefficient: R^2 = 84.70%–99.99%; standard deviation: SD = 0.0021 – 1.58). The desirability function-based optimization indicated that: J_{max} and τ_{tmax} are obtained for X_{1max} (200 ppm), X_{2max} (60% w/w) and X_{3min} (50 μm), for a desirability value of 0.93 and 0.81, respectively, while τ_{fmax} is obtained for X_{1max}, X_{2max} and X_{3max} (65 μm), for a desirability value of 0.93.

Keywords: Membrane process; Polymer inclusion membranes; Heavy metals; Competitive transport; Full-factorial design; Desirability function

1. Introduction

Membrane processes are increasingly reported for various applications in many industries, taking advantages of their selectivity, high surface area per unit volume, and their potential for controlling the level of contact and/or mixing between two phases [1,2]. In this context, separations using polymer inclusion membranes (PIMs) have gained attention during the last years due to their specific advantages such as effective carrier immobilization, ease of synthesis, versatility, and good mechanical properties [3–5]. PIMs are typically prepared by solution casting method with molding the polymer solution in a Petri dish or casting knife or membrane applicator on a glass surface [3]. They are a solid mixture usually composed of a base membrane skeleton (commonly poly(vinyl chloride) (PVC) or cellulose triacetate (CTA)), an extractant (carrier) and a plasticizer or modifier [6–10]. The carrier is essentially a complexing agent or an ion-exchanger, responsible for binding with the species of interest and transporting it across the PIM. This process relies on the concentration gradient of the species/carrier complex or ion-pair formed within the membrane, which acts as the driving force enabling transport across the membrane [8]. The base polymer provides the membrane with mechanical strength and the plasticizer provides elasticity and flexibility [5,8].

Compared with traditional supported liquid membranes (SLMs), whose major drawback is poor stability

* Corresponding author.

rendering them mostly impractical for many applications [5,8], PIMs have been reported as a potential separation technology to extract and transport several heavy metals (e.g., cobalt [11–13], nickel [12,14,15], zinc [16–19], chromium [3,7,20,21], lead [18,22], cupper [6,10,15], etc.). However, in spite of the progress made with these membranes, up to now all the researches about them have been conducted on a laboratory scale. Therefore, their commercial applications in a near future will depend on the transition of this research to a pilot or full-scale application. To this end, the understanding of the main variables that influence membrane behavior, transport efficiency and mechanisms within them is of relevant importance.

In this context, the aim of the present study was to study the competitive transport of 4 heavy metals species (Ni^{2+}, Co^{2+}, Cr^{3+} and Zn^{2+}) across CTA-based PIMs with polyethylene glycol (PEG) and tris(2-ethylhexyl) phosphate (TEHP) used as membrane components. In this research, several PIMs were synthesized according to a full factorial design methodology in order to investigate the effects of their composition (ratio PEG/CTA) and thicknesses along with the initial concentration of metals on 3 responses variables: the matter flux of every metal and the percentages of metals transferred and fixed. The purpose was mainly to elaborate mathematical models allowing a better understanding of the experimental results, and then, to optimize the process by using the desirability function approach.

2. Materials and methods

2.1. Membranes synthesis

Organic compounds: CTA, PEG, TEHP used as membrane components to prepare PIMs were purchased from Sigma-Aldrich (St. Louis, MO, USA). Chloroform was purchased from Carlo Erba, France.

The PIMs were prepared using solvent evaporation method [10,23,24]. Typically, 0.3 g CTA were dissolved in 30 mL of chloroform by stirring for 2.5 h at room temperature. PEG and the CTA solution were then mixed with a weight ratio of PEG/CTA varied from 10% to 60%. After vigorous stirring for 30 min, 0.3 mL of TEHP was added and the solution was stirred for 2 h at room temperature to obtain a homogenous solution. The resulting solution was then poured into glass Petri dishes (128 and 148 mm of diameters to obtain two different thicknesses: dimensions D_1 and D_2 (*cf.* Table 2), and chloroform was allowed to evaporate slowly at room temperature over night to yield a flexible, transparent and mechanically strong membranes. The obtained membranes were then carefully peeled off the dishes and cut to the required size for use in the transport cell. The thicknesses of the membranes (D_1 and D_2) were estimated from images of their cross-sections, obtained by scanning electronic microscopy at different locations.

2.2. Membranes characterization

Attenuated total reflectance Fourier-transform infrared (ATR-FTIR) spectra were recorded on a Nicolet iS5 spectrophotometer equipped with an iD7 ATR accessory (Thermo Fisher Scientific: Waltham, MA, USA). The infrared (IR) spectra of 4,000–400 cm^{-1} with a resolution of 4 cm^{-1} were determined by accumulating 32 scans. All original spectra were analyzed using OMNIC software.

The morphologies of the membranes were observed with an FEI Quanta 200 scanning electron microscope (Oregon, USA). The observations were carried out on the cross-section and upper surface of membranes before and after the experiments, to investigate their possibly morphological changes, and eventually the distribution of metals within them after an exposure time.

2.3. Experimental setup for the transport study

In the present study, in order to study the competitive transport of metals (Ni^{2+}, Co^{2+}, Cr^{3+} and Zn^{2+}) across the PIMs, batch experiments were conducted at room temperature (25°C), in a transport cell formed by two identical compartments (140 mL, each) separated by a membrane (Fig. 1). Both compartments containing the source and receiving solutions (deionized water) were kept under rigorous stirring for over 6 h. The transport process across PIMs involves essentially the exchanging of ionic species between these two compartments. At the end of the manipulation, a sample of each compartment is analyzed by atomic absorption spectroscopy to determine the concentration of metals. The apparatus used is a flame atomic absorption spectrophotometer AAnalyst 200 (PerkinElmer: Waltham, MA, USA). All measurements were made under the following conditions: air-acetylene flame, spectral bandwidth: 0.5 nm, lamp current: 10 mA, air flow rate: 10 L/min, acetylene flow rate: 2.5 L/min. Five separate readings were made for each solution at the wavelengths (nm): 213.86 for Zn, 357.9 for Cr, 240.7 for Co and 232 for Ni. The means of these measurements were used to calculate the concentrations.

All chemical reagents used were of analytical grade. Inorganic chemicals: $ZnCl_2$, $CoCl_2$ and $Cr_2(SO_4)_3$ were obtained from Sigma-Aldrich (St. Louis, MO, USA), $NiCl_2$ was purchased from Fulka (France). Stock solutions of diverse metals were prepared from the high purity compounds (99.9%) purchased from Sigma-Aldrich (St. Louis, MO, USA).

2.4. Experimental procedure according to a 2^3 full factorial design

A three-factor 2-level full factorial design: "2^3 FFD" was employed to evaluate the importance and interactions of 3 independent factors: the initial concentration of metals (X_1), carrier content (X_2: ratio mPEG/mCTA) and PIMs

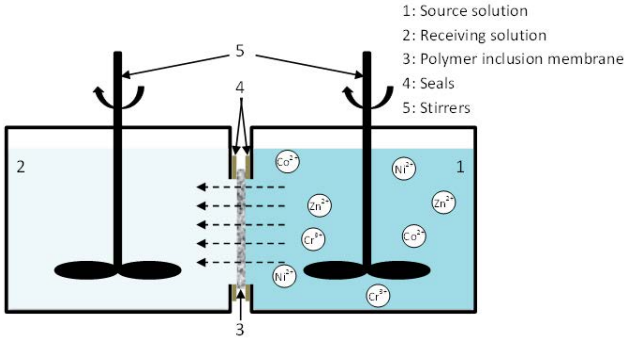

Fig. 1. Experimental device.

thickness (X_3). The response variables in this study were the matter flux 'J' through the PIMs, the percentage of metal ions transferred to the receiving compartment 'τ_t' and the percentage of metal ions fixed inside the PIMs 'τ_f'.

The individual matter flux through the PIMs, of each studied metal ion (Co^{2+}, Cr^{3+}, Ni^{2+}, Zn^{2+}) separately, is calculated by Eq. (1):

$$J_i = \frac{(\Delta n)_{i,RS}}{A \cdot \Delta t} \tag{1}$$

where i represents the index of heavy metal ions referring to Co, Cr, Ni and Zn, J_i (μmol/m²·s) the individual matter flux through the PIMs of the targeted metal ion, $(\Delta n)_{i,RS}$ the variation in the mole number in the receiving solution, A the exposed membrane area for the metals transport ($A = 11.33 \times 10^{-4}$ m²) and Δt is the experiment time (6 h).

The global matter flux of all metals is given by Eq. (2):

$$J_T = \frac{(\Delta n)_{T,RS}}{A \cdot \Delta t} \tag{2}$$

where $(\Delta n)_{T,RS}$ is the variation in the total mole number in the receiving solution.

The percentage of metal ions transferred through the PIMs is calculated by Eq. (3):

$$\tau_{t,i}(\%) = \frac{\left[M^{n+}\right]_{if,RS}}{\left[M^{n+}\right]_{i0,SS}} \times 100 \tag{3}$$

where i represents the index of metal ions referring to Co^{2+}, Cr^{3+}, Ni^{2+} and Zn^{2+}, $\tau_{t,i}(\%)$ the individual percentage of the targeted metal ion transferred through the PIMs (recovery factor), $[M^{n+}]_{if,RS}$ the final concentration in the receiving solution after 6 h processing and $[M^{n+}]_{i0,SS}$ is the initial concentration in the source solution.

The total percentage of metal ions transferred through the PIMs (total recovery factor) is given by Eq. (4):

$$\tau_{Tt}(\%) = \frac{\sum_1^4 \left[M^{n+}\right]_{if,RS}}{\sum_1^4 \left[M^{n+}\right]_{i0,SS}} \times 100 \tag{4}$$

The percentage of metal ions fixed inside the PIMs is calculated by Eq. (5):

$$\tau_{f,i}(\%) = \frac{\left[M^{n+}\right]_{i0,SS} - \left(\left[M^{n+}\right]_{if,RS} + \left[M^{n+}\right]_{if,SS}\right)}{\left[M^{n+}\right]_{i0,SS}} \times 100 \tag{5}$$

where $\tau_{f,i}$ (%) is the individual percentage of the targeted metal ion fixed inside the PIMs and $[M^{n+}]_{if,SS}$ the final concentrations in the source solution.

The total percentage of metal ions fixed inside the PIMs is given by Eq. (6):

$$\tau_{Tf}(\%) = \frac{\sum_1^4 \left[M^{n+}\right]_{i0,SS} - \left(\sum_1^4 \left[M^{n+}\right]_{if,RS} + \sum_1^4 \left[M^{n+}\right]_{if,SS}\right)}{\sum_1^4 \left[M^{n+}\right]_{i0,SS}} \times 100 \tag{6}$$

The advantages and disadvantages of the designs of experiment are well known: minimize the number of experiments, and therefore reduce costs and time, and above all, carrying out the processing and analysis of experimental results in a much more efficient way, leading always to an empirical modeling of responses on one side, but also to simulation by the technique of response surfaces [25–27]. Furthermore, the use of the FFD methodology in this work aimed to identify the important factors in the membrane process while studying eventual interactions between them, and optimizing them. The design determines the effect of each factor on each response as well as how the effect of each factor varies with the change in the level of the other factors, that is, interactions. If there is interaction between two or more factors, that is, factors are interdependent; it means that the level of one factor changes the effect of other factors on a specific response [25]. It should be noted that the factors used in this work have never been investigated simultaneously using factorial designs, and that they were chosen for their effects, as determined in several previous works using one variable-at-a-time experimental procedures [5,8].

In two-levels FFD, each factor has two levels, a 'high level' or '+1' and a 'low level' or '–1'. If there are k factors in a process, two-level FFD has 2^k runs [26]. Therefore, the present 2^3 FFD is yielded with 8 experiments corresponding to the factorial points. When the lower level of a factor is represented by –1 and the upper level is represented by + 1, two important changes occur: (1) the center of the measurements moves and (2) the measurement units change. These two changes involve the introduction of new variables called centered and scaled variables (CSV) [25–27]. Centering refers to the change of origin, and scaling refers to the change of units. These new variables are also commonly called coded variables or coded units. The advantage to using coded units lies in their power to present designed experiments in the same way, regardless of the chosen study domains and regardless of the factors. Seen this way, design of experiments theory is quite generalizable [26,27]. The three independent variables are coded according to Eq. (7) [25–27]:

$$x_i = \frac{X_i - X_{i,0}}{\Delta X_i} \tag{7}$$

where i = 1–3 referring to the three independent factors, x_i and X_i are respectively the dimensionless and the actual values of independent variable i, $X_{i,0}$ the actual value of independent variable i at central point and ΔX_i the step change of X_i corresponding to a unit variation of the dimensionless value.

The ranges of variation of the 3 studied factors are given in Table 1 both in real and coded values.

Table 2 shows the experimental design matrix of the followed 2^3 FFD. The experiments were carried out in randomized run order to determine the effect of the factors on the 3 characteristic responses: J, τ_t and τ_f. Table 2 collates also the designation of the different membranes synthesized in this study, according to the followed factorial design, that is, two membranes with different carrier contents (Memb1 and Memb2), each with 2 different thicknesses (D_1 and D_2).

Table 1
Factors and their levels used in the 2^3 FFD

Independent factors	Levels		
	Low level (–1)	Center (0)	High level (+1)
Metals concentration: X_1 (mg/L)	20	110	200
Carrier ratio: X_2 (w/w %)	10	35	60
Membrane thickness: X_3 (μm)	50 (D_1)	57.5	65 (D_2)

Table 2
Design matrix with coded and real values of factors – designation of the synthesized membranes

Run (Ref.)	Coded factors			Processing conditions			Membranes' designation
	X_1	X_2	X_3	X_1 (mg/L)	X_2 (w/w %)	X_3 (μm)	
Run 1	–	–	–	20	10	50	Memb1-D_1
Run 2	+	–	–	200	10	50	Memb1-D_1
Run 3	–	+	–	20	60	50	Memb2-D_1
Run 4	+	+	–	200	60	50	Memb2-D_1
Run 5	–	–	+	20	10	65	Memb1-D_2
Run 6	+	–	+	200	10	65	Memb1-D_2
Run 7	–	+	+	20	60	65	Memb2-D_2
Run 8	+	+	+	200	60	65	Memb2-D_2

The studied responses are related to the three independent variables and their interaction terms according to the first-order model expressed in Eq. (8) [25–27]:

$$Y = \alpha_0 + \sum_1^n \alpha_i \cdot x_i + \sum_1^n \alpha_{ij} \cdot x_i x_j \quad (8)$$

where α coefficients are the regression model constants: α_0 is the interception coefficient (average value of the results), α_i the linear terms and α_{ij} the interaction terms. x_i and x_j are the coded values of the independent variables.

To estimate the significance of the proposed models, the statistical calculations (*t*-test, *F*-test, analysis of variance (ANOVA)) and the surface responses were performed by using the analysis design procedure of JMP software (8^{th} version). Contour plots were generated by assigning constant values to one variable and then fitting the solution to Eq. (8).

The problem here involves conflicting responses that must be optimized simultaneously, because their separate analysis may result in incompatible solutions. Indeed, it is about a competitive transfer of four metal ions, where the maximization of the flux of a metal ion will be done to the detriment of the other metal ions. On the other hand, a greater amount of metal ions fixed inside membranes indicates a better matter transfer, but paradoxically, a greater amount fixed means a lower transfer to the recovery compartment. That's the reason why the desirability function approach is used in this work to optimize the process; it's indeed one of the most widely used methods in industry for the optimization of multiple response processes [27,29,30]. It is based on the idea that the quality of a process that has multiple quality characteristics, with one of them outside of some desired limits, is completely unacceptable [29]. The method finds operating conditions that provide the most desirable response values [29,30]. Indeed, the desirability function involves transformation of each estimated response variable Y_i to a desirability value d_i; where $0 \le d_i \le 1$. The value of d_i increases as the "desirability" of the corresponding response increases. The individual desirability's are then combined using the geometric mean in a single value D ($0 \le D \le 1$) which gives the overall assessment of the desirability of the combined response levels. D will then increases as the balance of the responses becomes more favorable [30].

3. Results and discussions

3.1. Study and characterization of the synthesized membranes

Table 2 gathers the designation and characteristics of the different membranes synthesized in this study, according to the followed 2^3 FFD. The differences between the synthesized membranes are their thicknesses and the percentage of PEG they contain. Thereby, two membranes with different PEG contents were synthesized (Memb1 and Memb2), each with two different thicknesses (D_1 and D_2).

3.1.1. Fourier-transform infrared spectroscopy

In this study, ATR-IR analysis was used to characterize PIMs with the aim to elucidate the specific interactions between the membrane components. Fig. 2 presents the spectra of the four synthesized PIMs: Memb1-D_1, Memb1-D_2, Memb2-D_1 and Memb2-D_2. From first sight, it can be concluded that membranes of the same composition have identical spectra: Memb1-D_1 and Memb1-D_2 (Fig. 2a); Memb2-D_1 and Memb2-D_2 (Fig. 2b), which indicates that the followed technique of synthesizing is quite repetitive and that the size of the Petri dishes, which sets the thickness of the membranes, does not affect directly their compositions.

The main feature of the PIMs spectra shown in Fig. 2 displays a number of absorption peaks, noticed around 1,020; 1,220; 1,740; 2,850; 2,930; 1,360; 1,440 and 3,440 cm^{-1}. The strong peak located at 1,740 cm^{-1} is attributed to C=O in carboxylic groups for CTA while the two less strong peaks located around 2,850–2,930 cm^{-1} are attributed to aliphatic C–H groups for both TEHP and PEG, and the wide band centered at 3,400 cm^{-1} is assigned to O–H bond stretching (PEG and CTA). The strong peaks around 1,020 and 1,230 cm^{-1} correspond to the stretching mode of C–O–C groups from TEHP, PEG and CTA. The narrow peaks at 1,360–1,430 cm^{-1} may be attributed to the halogenated C–H or other vibrations mode of the carbonated skeleton. Finally, Fig. 2c and d show only a small difference between Memb1 and Memb2 located at the band centered around 3,400 cm^{-1} and attributed to the O–H bond stretching. The ATR-IR spectra shown in Fig. 2 confirm the presence of both TEHP and PEG in the polymer matrix (CTA) but do not reveal if some new

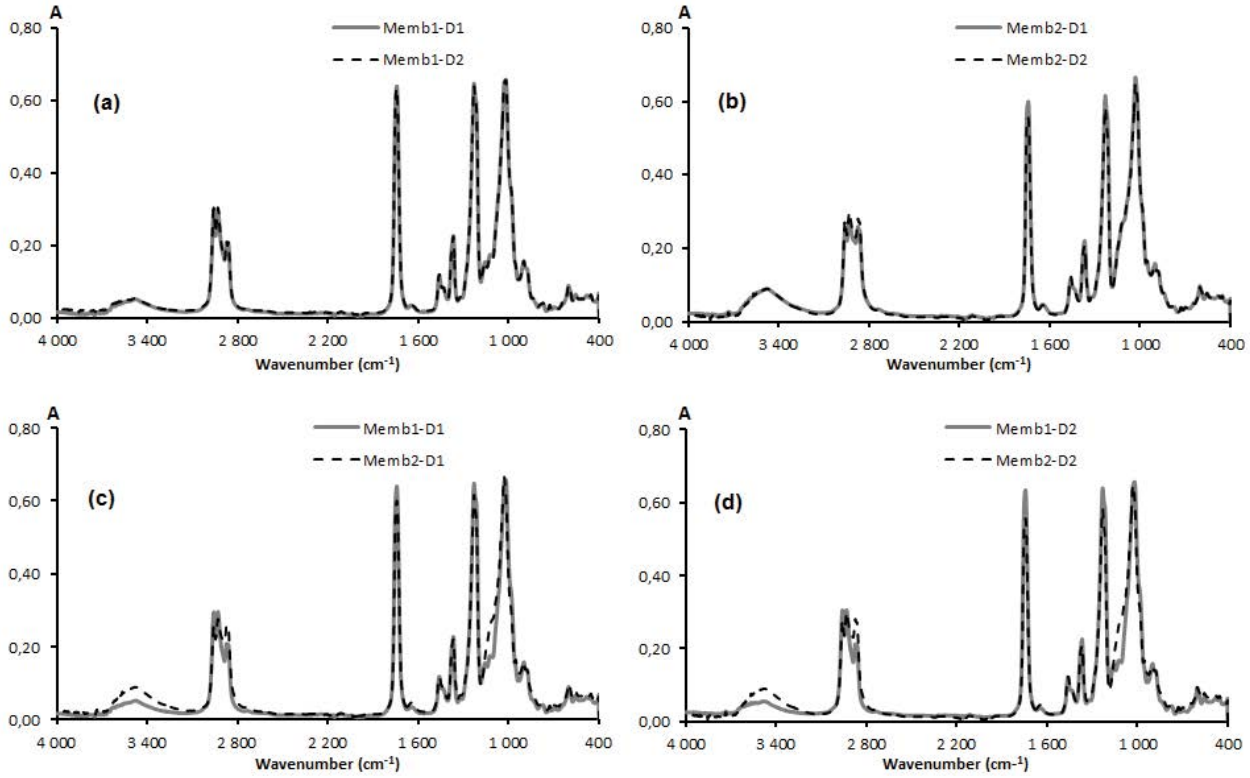

Fig. 2. ATR-IR spectra of PIMs. (a) Membrane 1 (two different thicknesses), (b) membrane 2 (two different thicknesses), (c) membranes 1 and 2 (thickness D_1) and (d) membranes 1 and 2 (thickness D_2).

covalent bonds occur between the PIMs components. From the literature review reported by Nghiem et al. [5], several FTIR studies have revealed no signs of covalent bond formation between the carrier, plasticizer and the base membrane skeleton and that there is a form of secondary bonding such as hydrophobic, van der Waals or hydrogen bonds which happens between the PIMs components.

3.1.2. Scanning electronic microscopy

The morphology of synthetic membranes is impressively complex, diverse, and irregular. It depends on the material used and the mode of preparation [28]. In the case of PIMs, the microstructure is an important parameter because it determines the distribution of carriers in the polymer matrix and by the way affects the membrane transport efficiency. In this study, scanning electron microscopy (SEM) analyses were performed on membranes before and after transport study experiments and were also used to estimate the thicknesses of the membranes.

The SEM images of the upper surface and the cross-section of the two synthesized membranes (Memb1 and Memb2) are given in Fig. 3a and b, respectively. It can be noticed the total lack of pores which confirms the dense nature of the membranes. Indeed, the addition of plasticizer clogs the existent pores as reported in previous studies cited by Nghiem et al. [5]. The principal role of plasticizers is to increase the membrane softness and flexibility by penetration between polymer molecules to "neutralize" the polar groups of the polymer with its own polar groups or to merely increase the distance between the polymer molecules and hence reduce the strength of the intermolecular forces [5].

The SEM images of the upper surface and the cross-section of Memb1 and Memb2 after being used in the transport study experiments are given in Fig. 3c and d, respectively. The major difference that can be observed at first sight with the images of the membranes prior to use are those points and spots that appear fluorescent and which can be attributed to the different metal ions transported across the PIMs. In addition, it can be seen on these images that the metal ions are scattered over the entire thickness of the membranes, which confirms their mobility within them.

3.2. Statistical analysis of the transport through PIMs – models fitting

3.2.1. Modeling of the matter fluxes crossing the PIMs

Table 3 presents the concentrations of Ni, Co, Cr and Zn (mg/L) in both source and receiving solutions after 6 h processing. The matter fluxes through the PIMs calculated using Eqs. (1) and (2) are given in Table 4. The maximum concentration in the receiving solution was obtained in run 4 for all metals; this corresponds to the maximum of X_1 (initial concentration of metals) and X_2 (the carrier ratio) and the minimum of X_3 (the membrane thickness). This means that the carrier ratio and the gradient of concentration have a positive effect on the transfer of metallic ions, in different proportions depending on the metal, while

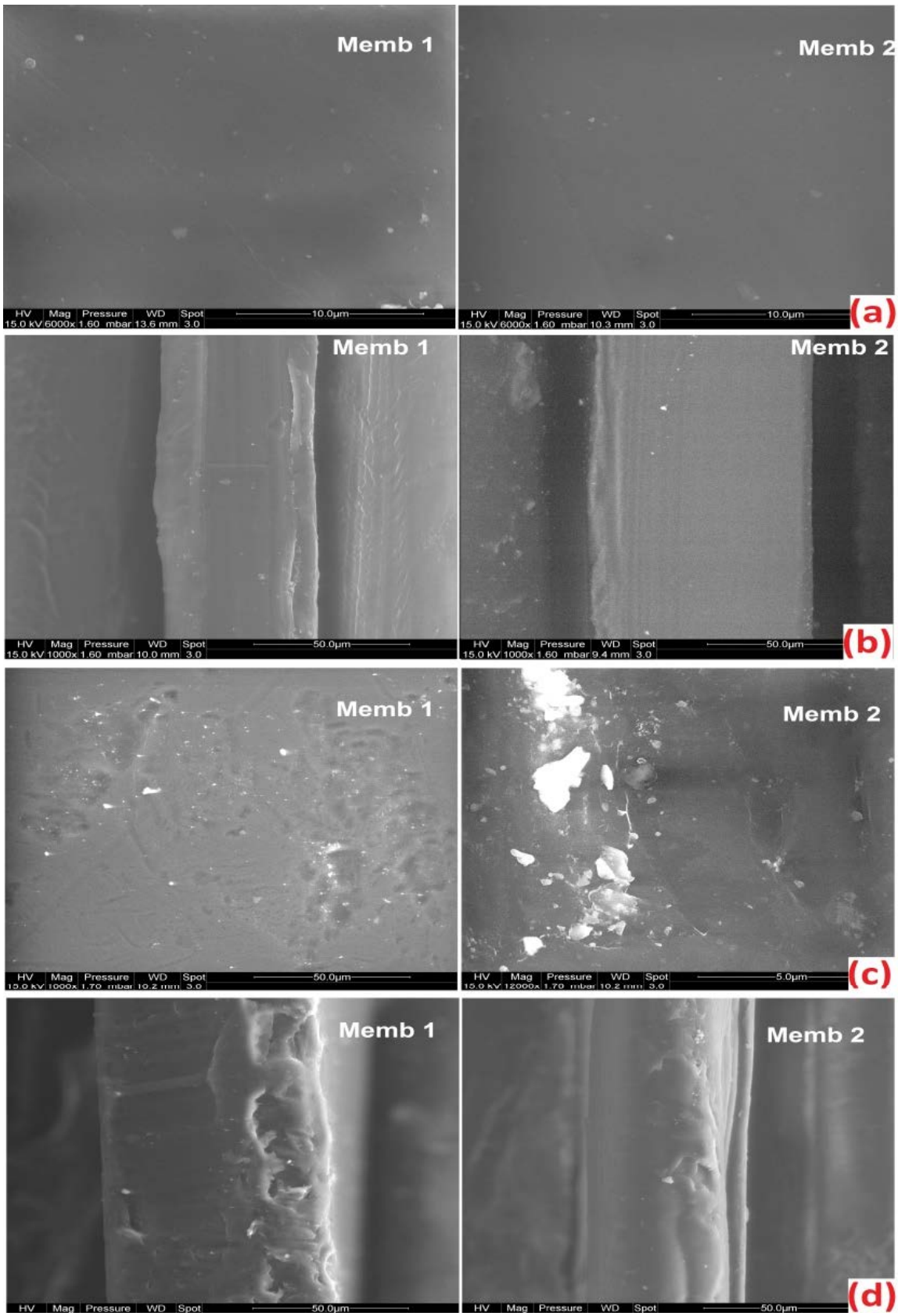

Fig. 3. Scanning electron microscopy pictures of the membranes: – before being used in the transport study: (a) upper surface, (b) cross-section – after the experiments: (c) upper surface and (d) cross-section.

Table 3
Metals concentrations (mg/L) in both source and receiving compartments, measured by flame atomic absorption spectroscopy (FAAS) after 6 h processing

Run (Ref.)	Coded factors			Metals concentration (mg/L)							
				Ni		Co		Cr		Zn	
	X_1	X_2	X_3	SS[a]	RS[b]	SS[a]	RS[b]	SS[a]	RS[b]	SS[a]	RS[b]
Run 1	–	–	–	14.625	0.423	18.312	0.176	16.806	0.248	16.711	0.555
Run 2	+	–	–	65.520	5.980	91.178	0.322	83.634	0.606	80.010	5.870
Run 3	–	+	–	13.366	1.230	18.077	0.283	16.196	0.716	15.062	2.122
Run 4	+	+	–	63.009	7.011	89.767	1.103	80.503	2.797	76.232	8.128
Run 5	–	–	+	13.646	0.330	17.416	0.120	15.826	0.800	15.441	1.095
Run 6	+	–	+	62.110	4.320	83.745	0.245	81.895	0.675	75.200	3.350
Run 7	–	+	+	12.814	0.830	16.783	0.189	16.205	0.349	14.399	2.067
Run 8	+	+	+	56.547	6.023	81.665	0.905	76.075	1.995	67.755	7.115

[a]Source solution;
[b]Receiving solution.

the thickness of the membrane has a negative effect since it delays the transfer.

The corresponding maximum fluxes found in run 4 were 0.68, 0.11, 0.31 and 1.42 μmol/m²·s, respectively for Ni, Co, Cr and Zn, while the total matter flux was equal to 2.52 μmol/m²·s. The results in Table 4 showed also that the selectivity order of heavy metal ions across the synthesized PIMs is Zn > Ni > Cr > Co. The mean flux of Zn is found to be equal to two times that of Ni, five times that of Cr and sixteen times that of Co.

Our results on the membranes' selectivity towards the metal ions are in good agreement with the results reported in the literature as listed in Table 5, for PIMs of different compositions. In essence, the selective separation of metal ions by PIM is attributed to the type of extractant involved in the extraction reaction between the feed solution and the PIM membrane, as well as the diffusion through it.

The significance of linear terms and interaction terms through variance analysis (ANOVA) are given in Table 6 for individual and total matter fluxes. Based on *p*-values, the significant effects ($p < 0.05$) of linear and interaction terms on matter fluxes depend on the considered metal: the initial concentration of metals (X_1) has a significant effect whatever the metal; for Cr all effects are significant except that of the membrane thickness (X_3) and for Co, X_1, X_2 and X_1X_2 have significant effects. For all metals, X_1 had the most significant effect followed by X_2 according to this order: $X_1 > X_2 > X_3 > X_1X_3 > X_1X_2 > X_2X_3$ for Ni; $X_1 > X_2 > X_1X_2 > X_3 > X_2X_3 > X_1X_3$ for Co; $X_1 > X_2 > X_1X_2 > X_2X_3 > X_1X_3 > X_3$ for Cr; $X_1 > X_2 > X_1X_3 > X_1X_2 > X_3 > X_2X_3$ for Zn; $X_1 > X_2 > X_1X_2 > X_1X_3 > X_3 > X_2X_3$ for all metals (total matter flux). Moreover, the interaction X_1X_2, that is, between the initial concentration

Table 4
Matter flux of metals through the PIMs

Run (Ref.)	Coded factors			Mater flux 'J_i' of metal ions (μmol/m²·s)				
	X_1	X_2	X_3	Ni	Co	Cr	Zn	Total
Run 1	–	–	–	0.041	0.017	0.027	0.097	0.183
Run 2	+	–	–	0.583	0.031	0.067	1.027	1.707
Run 3	–	+	–	0.120	0.027	0.079	0.371	0.597
Run 4	+	+	–	0.683	0.107	0.308	1.422	2.519
Run 5	–	–	+	0.032	0.012	0.088	0.191	0.323
Run 6	+	–	+	0.421	0.024	0.074	0.586	1.105
Run 7	–	+	+	0.081	0.018	0.038	0.362	0.499
Run 8	+	+	+	0.587	0.088	0.219	1.245	2.139

Table 5
Selectivity of PIMs towards different metal ions species

PIMs' composition: base polymer/extractant/plasticizer	Metal ion selectivity order	References
CTA/PEG/TEHP	$Zn^{2+} > Ni^{2+} > Cr^{3+} > Co^{2+}$	Present study
CTA/1-alkyltriazole 1–9/o-NPPE	$Pd^{2+} > Zn^{2+} > Ni^{2+}$	[14]
CTA/EDAB-acac/o-NPPE	$Zn^{2+} > Cr^{3+} > Ni^{2+}$	[31]
CTA/RILC8_Br/NPOE	$Cd^{2+} > Zn^{2+} > Pb^{2+} >> Cu^{2+}$	[32]
CTA/calixresorcin[4]arene/o-NPOE, o-NPPE, DOA	$Pb^{2+} > Cd^{2+} > Zn^{2++}$	[33]
CTA/TRIA-8/ONPOE	$Cu^{2+} > Ni^{2+} > Co^{2+}$	[34]
PVC/c-TBP	$Li^{+} > Mg^{2+}$	[35]
Cross-linked GPO/BMIMCl, 12C4, and ZIF-8	$Li^{+} > Na^{+}$, K^{+}, Ca^{2+}, and Mg^{2+}	[36]

Table 6
Statistical analysis of results concerning the matter fluxes

Parameter	Ni			Co			Cr			Zn			Total		
	MC[a]: α_i	SE[b]	*p*-value	MC[a]: α_i	SE[b]	*p*-value	MC[a]: α_i	SE[b]	*p*-value	MC[a]: α_i	SE[b]	*p*-value	MC[a]: α_i	SE[b]	*p*-value
Constant	0.3185	0.012	0.024*	0.0405	0.001	0.016*	0.1125	0.00075	0.004*	0.6626	0.046	0.044*	1.1340	0.058	0.032*
X_1	0.2500	0.012	0.031*	0.0220	0.001	0.029*	0.0545	0.00075	0.009*	0.4074	0.046	0.071*	0.7335	0.058	0.050*
X_2	0.0493	0.012	0.152	0.0195	0.001	0.033*	0.0485	0.00075	0.010*	0.1874	0.046	0.153	0.3045	0.058	0.119
X_3	–0.0383	0.012	0.194	–0.0050	0.001	0.126	–0.0078	0.00075	0.061	–0.0666	0.046	0.384	–0.1175	0.058	0.290
X_1X_2	0.0173	0.012	0.387	0.0155	0.001	0.041*	0.0480	0.00075	0.010*	0.0761	0.046	0.345	0.1570	0.058	0.223
X_1X_3	–0.0263	0.012	0.273	–0.0015	0.001	0.374	–0.0128	0.00075	0.037*	–0.0879	0.046	0.306	–0.1280	0.058	0.269
X_2X_3	0.0045	0.012	0.772	–0.0020	0.001	0.295	–0.0248	0.00075	0.019*	0.0201	0.046	0.737	–0.0020	0.058	0.978
R^2	0.9979			0.9991			0.9999			0.9905			0.9952		
Adj. R^2	0.9851			0.9938			0.9995			0.9335			0.9664		
R-SD[c]	0.0339			0.0028			0.0021			0.1297			0.1626		

[a]Model coefficients based on Eq. (8);
[b]Standard error;
[c]Residual standard deviation;
*Significant effect: $p < 0.05$.

and the carrier ratio was statistically significant, indicating an antagonistic effect between these variables on responses parameters. In addition, the interaction X_1X_3, that is, between the initial concentration and the membrane thickness was also significant with a negative effect on matter fluxes. The regression analysis was carried out to fit experimental data, using mathematical models, aiming at an optimal region for the responses parameters. The models developed for each response are described by Eqs. (9)–(13):

$$J_{Ni} = 0.3185 + 0.25x_1 + 0.0493x_2 - 0.0383x_3 + 0.0173x_1x_2 - 0.0263x_1x_3 + 0.0045x_2x_3 \quad (9)$$

$$J_{Co} = 0.0405 + 0.0220x_1 + 0.0195x_2 - 0.0050x_3 + 0.0155x_1x_2 - 0.0015x_1x_3 - 0.0020x_2x_3 \quad (10)$$

$$J_{Cr} = 0.1125 + 0.0545x_1 + 0.0485x_2 - 0.0078x_3 + 0.0480x_1x_2 - 0.0128x_1x_3 - 0.0248x_2x_3 \quad (11)$$

$$J_{Zn} = 0.6626 + 0.4074x_1 + 0.1874x_2 - 0.0666x_3 + 0.0761x_1x_2 - 0.0879x_1x_3 + 0.0201x_2x_3 \quad (12)$$

$$J_T = 1.1340 + 0.7335x_1 + 0.3045x_2 - 0.1175x_3 + 0.1570x_1x_2 - 0.1280x_1x_3 - 0.0020x_2x_3 \quad (13)$$

The statistics used to test the adequacy of the models at confidence level of 95% are summarized in Table 6. The determination coefficient (R^2) measures the proportion of total variability explained by the model, while the adjusted-R^2 is a statistic that is adjusted for the "size" of the model, that is, number of factors. Therefore, the adjusted R^2 can decrease if insignificant factors are added to the model [26]. From Table 6, it can be seen that adjusted R^2 were higher than 0.93 even by considering the insignificant factors. Furthermore, the values of R^2 for all responses were systematically higher than 0.99 and standard deviation less than 3% for Ni, Co and Cr (not significant) and between 12 and 16% for Zn and the total matter flux. Thus, all the statistics given in Table 6 indicate that the estimated model for each response fits the experimental data adequately.

Fig. 4a–c depicts via three-dimensional (3D) response surface plot, the matter fluxes mapped against two experimental factors while the third factor was set constant at its central value (*cf.* Table 1). It can be seen from these figures that X_1 and X_2 have a positive effect on the matter flux while X_3 has a negative effect. Besides, Fig. 4a shows that the interaction between X_1 and X_2 is important for Co and Cr. Indeed, the carrier ratio favored the matter fluxes crossing the PIMs for all metals, but mainly when the initial concentration was at its high level (200 ppm) for Co and Cr. In the same way, the initial concentration favored the matter fluxes crossing the PIMs for all metals, but mainly when the carrier ratio was at its high level (60% w/w) for Co and Cr. For the other metals, it can be concluded from Fig. 4a that the effect of the initial concentration is higher than that of the carrier ratio. This shows that the concentration gradient on both sides of the membrane is the main driving force of the transfer although the carrier concentration within the membrane matrix also has a positive effect.

From Fig. 4b and c it can be seen that the membrane thickness (X_3) has a negative effect on the matter fluxes regardless of the levels of X_1 and X_2, and that this effect is slightly different depending on the levels of these factors and the interactions between them. For example, at high concentrations of metal ions (200 ppm) and high carrier contents (60% w/w), when X_3 increases from 50 to 65 μm, the matter fluxes decrease by: 15.98%, 17.14%, 28.66% and 18.65%,

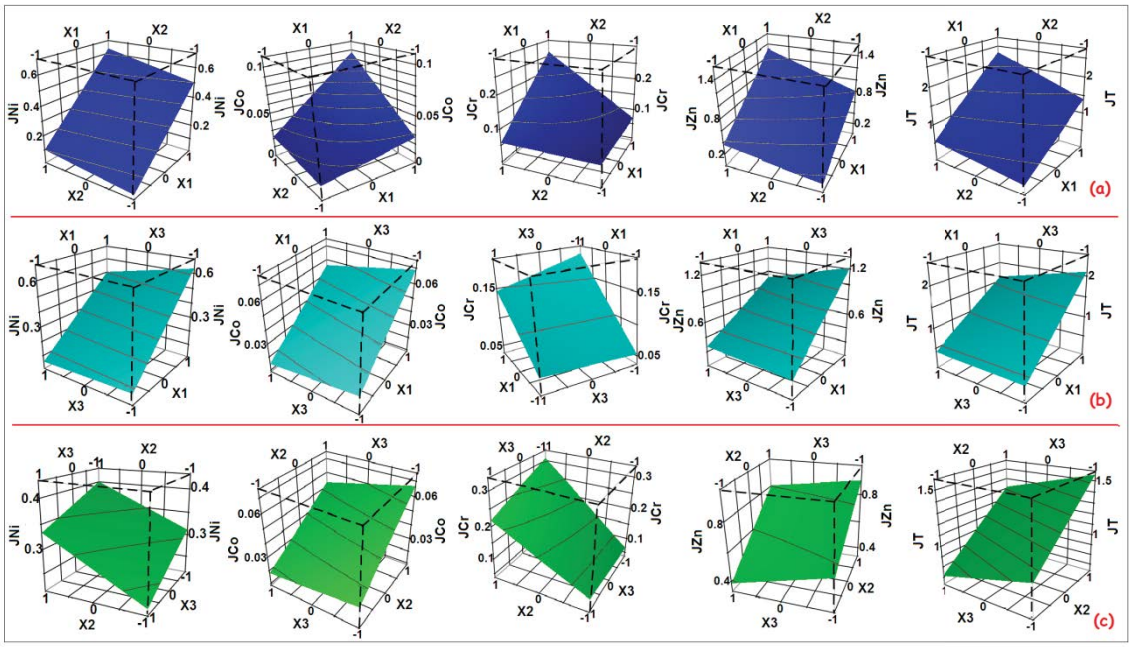

Fig. 4. 3D-plot of the response surfaces for the metals fluxes vs.: (a) X_1 and X_2, (b) X_1 and X_3, and (c) X_2 and X_3.

respectively for Ni, Co, Cr and Zn, while the global matter flux decreases by 18.66%. On the other hand, for a low carrier content (10% w/w), and still at high initial concentrations of metal ions, when X_3 increases from 50 to 65 μm, the metal fluxes decrease more strongly indicating the important role of the carrier: decrease of 24.74% for Ni, 28.12% for Co, 10.81% for Cr, 34.75% for Zn and 29.14% for the global matter flux. Finally, the shape of the response surfaces given in Fig. 4 clearly indicates that the effect of the membrane thickness is the less significant on the matter fluxes and that the interaction between X_1 and X_2 greatly affects it and therefore plays a major role in metal ions transport.

The more favorable situation to obtain a maximal flux for each metal is obtained by the desirability approach, represented in Fig. 5. The favorable situation here corresponds to a high initial concentration for each metal (200 ppm), a high ratio of the carrier in the matrix of the membrane (60% w/w) and a low thickness (50 μm), for a desirability value of 0.93 and the following predicted responses: J_{Ni} = 0.695 μmol/m²·s; J_{Co} = 0.106 μmol/m²·s; J_{Cr} = 0.309 μmol/m²·s; J_{Zn} = 1.468 μmol/m²·s; J_T = 2.577 μmol/m²·s.

3.2.2. Modeling of the amount of metal ions transferred through the PIMs

Table 7 presents the percentages of Ni, Co, Cr and Zn transferred to the receiving solutions after 6 h processing, calculated by Eqs. (3) and (4). The results showed a maximum percentage transferred to the receiving solution obtained in run 3 for Zn (10.61%), run 4 for Ni (7.01%) and Co (5.51%) and run 5 for Cr (4.00%). These results showed then a divergence from a metal ion to another making the understanding of the linear effects of the studied parameters quite difficult at first sight.

The results in Table 7 showed also that the transfer order of heavy metal ions across the synthesized PIMs is Zn > Ni > Cr > Co. The average percentage of transferred Zn found to be equal to 6.71% is one and a half times that of Ni (4.67%) and three times those of Cr and Co (2.08%).

Table 8 gathers the results of the modelization of the percentage of metal ions transferred through PIMs and their statistical analysis (ANOVA). Based on *p*-values, except for Co for which X_1, X_2 and X_1X_2 have significant effects, the effects of linear and interaction terms are not significant for the other metal ions at a confidence level of 95%. The order of significance of the effects is random and shows a lot of difference between metals: $X_1 > X_2 > X_3 > X_1X_2 > X_2X_3 > X_1X_3$ for Ni; $X_1 > X_2 > X_1X_2 > X_3 > X_2X_3 > X_1X_3$ for Co; $X_2X_3 > X_1 > X_2 > X_1X_2 > X_1X_3 > X_3$ for Cr; $X_2 > X_1X_2 > X_1X_3 > X_1 > X_2X_3 > X_3$ for Zn; $X_2 > X_2X_3 > X_1X_3 > X_3 > X_1X_2 > X_1$ for all metals (total percentage transferred). Moreover, some interactions seems more important from a metal to another as depicted in Table 8.

The models developed to fit experimental data for each response are described by Eqs. (14)–(18):

$$\tau_{t,Ni} = 4.6750 + 1.1575x_1 + 1.1575x_2 - 0.6400x_3 - 0.4750x_1x_2 - 0.0225x_1x_3 - 0.1075x_2x_3 \quad (14)$$

$$\tau_{t,Co} = 2.0900 + 1.1300x_1 + 1.0100x_2 - 0.2650x_3 + 0.7900x_1x_2 - 0.0750x_1x_3 - 0.1000x_2x_3 \quad (15)$$

$$\tau_{t,Cr} = 2.0800 - 0.5600x_1 + 0.4500x_2 + 0.0225x_3 + 0.4300x_1x_2 - 0.2075x_1x_3 - 0.6825x_2x_3 \quad (16)$$

$$\tau_{t,Zn} = 6.7075 - 0.5900x_1 + 2.3425x_2 - 0.1375x_3 - 0.8350x_1x_2 - 0.7450x_1x_3 - 0.1825x_2x_3 \quad (17)$$

$$\tau_{t,T} = 3.5650 - 0.0375x_1 + 1.0600x_2 - 0.2200x_3 - 0.2025x_1x_2 - 0.2275x_1x_3 - 0.2550x_2x_3 \quad (18)$$

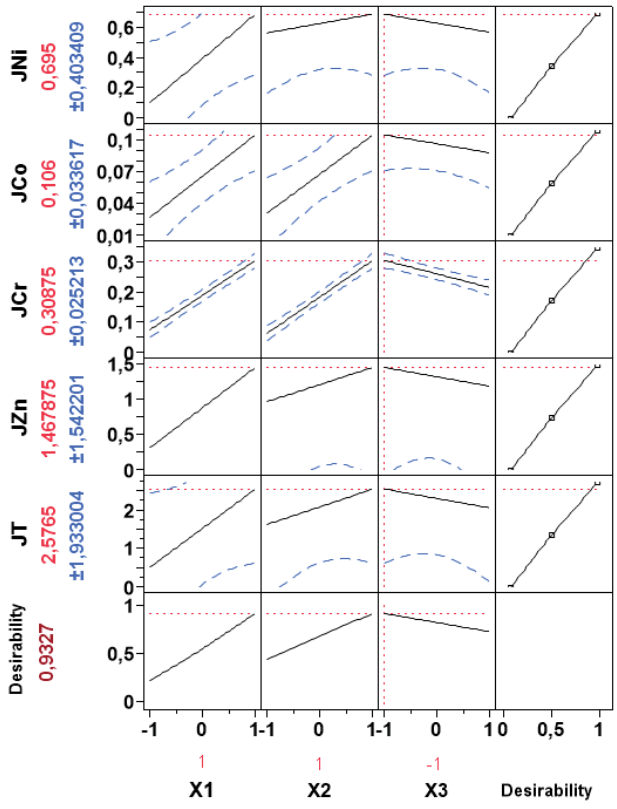

Fig. 5. Desirability function for the optimization of the matter fluxes of metal ions.

Table 7
Percentage of metals transferred to the receiving compartment

Run (Ref.)	Coded factors			Amount of transferred metals (%)				
	X_1	X_2	X_3	Ni	Co	Cr	Zn	Total
Run 1	–	–	–	2.12	0.88	1.24	2.77	1.75
Run 2	+	–	–	5.98	1.61	0.61	5.87	3.19
Run 3	–	+	–	6.15	1.42	3.58	10.61	5.44
Run 4	+	+	–	7.01	5.51	2.80	8.13	4.76
Run 5	–	–	+	1.65	0.60	4.00	5.47	2.93
Run 6	+	–	+	4.32	1.23	0.67	3.35	2.15
Run 7	–	+	+	4.15	0.94	1.74	10.34	4.29
Run 8	+	+	+	6.02	4.53	2.00	7.12	4.01

Table 8
Statistical analysis of results concerning the percentage of metals transferred through PIMs

Parameter	Ni			Co			Cr			Zn			Total		
	MC[a]: α_i	SE[b]	*p*-value	MC[a]: α_i	SE[b]	*p*-value	MC[a]: α_i	SE[b]	*p*-value	MC[a]: α_i	SE[b]	*p*-value	MC[a]: α_i	SE[b]	*p*-value
Constant	4.6750	0.275	0.037*	2.0900	0.050	0.015*	2.0800	0.467	0.141	6.7075	0.560	0.053	3.5650	0.328	0.058
X_1	1.1575	0.275	0.148	1.1300	0.050	0.028*	–0.5600	0.467	0.443	–0.5900	0.560	0.483	–0.0375	0.328	0.927
X_2	1.1575	0.275	0.148	1.0100	0.050	0.031*	0.4500	0.467	0.512	2.3425	0.560	0.149	1.0600	0.328	0.191
X_3	–0.6400	0.275	0.258	–0.2650	0.050	0.119	0.0225	0.467	0.969	–0.1375	0.560	0.847	–0.2200	0.328	0.623
X_1X_2	–0.4750	0.275	0.334	0.7900	0.050	0.040*	0.4300	0.467	0.527	–0.8350	0.560	0.376	–0.2025	0.328	0.647
X_1X_3	–0.0225	0.275	0.948	–0.0750	0.050	0.374	–0.2075	0.467	0.734	–0.7450	0.560	0.410	–0.2275	0.328	0.613
X_2X_3	–0.1075	0.275	0.763	–0.1000	0.050	0.295	–0.6825	0.467	0.382	–0.1825	0.560	0.799	–0.2550	0.328	0.579
R^2	0.9778			0.9992			0.8470			0.9579			0.9254		
Adj. R^2	0.8444			0.9942			0.7066			0.7055			0.7780		
R-SD[c]	0.7778			0.1414			1.3222			1.5839			0.9263		

[a]Model coefficients based on Eq. (8);
[b]Standard error;
[c]Residual standard deviation;
*Significant effect: $p < 0.05$.

The statistics used to test the adequacy of the models at confidence level of 95% are summarized in Table 8. The determination coefficient (R^2) varied from 84.70% for Cr to 99.92% for Co, and was up to 90% for the other responses, which suggests that the predicted models reasonably represent the observed values and therefore the responses were sufficiently explained by the models. Indeed, it is suggested that for a good fit model, R^2 should be close to 1 and should be at least 0.80 [25].

Fig. 6a–c depicts via 3D response surface plot, the percentage of transferred metal ions vs. two experimental factors while the third factor is kept constant at its central value (*cf.* Table 1).

It can be seen from these figures that X_2 had always a positive effect on all responses, while X_3 had a negative effect whatever the metal. Thus, it can be concluded that the carrier used in this work (PEG) is perm selective for all studied metal ions and that the membrane thickness does not favor, as expected, the metal ions transfer. Besides, Fig. 6a shows that the interaction between X_1 and X_2 is important; the carrier ratio (X_2) favored the transfer through the PIMs for all metal ions, but mainly when the initial concentration was at its low level (20 ppm) for Ni, Cr and Zn, and in the same way, the initial concentration favored the matter fluxes crossing the PIMs, but mainly when the carrier ratio was at its low level (10% w/w) for Ni and Cr. It can then be concluded from Fig. 6a that the effect of the carrier ratio is higher than that of the initial concentration for the transfer of ions across the PIMs.

From Fig. 6b it can be seen that the membrane thickness (X_3) has a negative effect on the amount of metal ions transferred through the PIMs, for all studied metals and regardless of the level of X_1. It can also be seen in this figure that the interaction between X_1 and X_3 is negligible, that is, the level of X_1 do not change the effect of X_3 on the quantity of metal ions transferred.

Finally, Fig. 6c shows that the interaction between X_2 and X_3 is negligible except for Cr, for which the level of X_2 modifies the effect of X_3 on the amount of transferred Cr^{3+}. Indeed, at a minimal ratio of the carrier (10% w/w), the effect of X_3 is almost constant on it, but at a high value of X_2, the effect of X_3 is significant and negative.

The use of the desirability approach to optimize the process in order to have a maximum of each metal ion transferred through the membrane, towards the receiving compartment, is represented in Fig. 7.

The operating conditions that provide the "most desirable" response values, that is, a maximum percentage transferred, correspond to a high initial concentration for each metal (200 ppm), a high ratio of the carrier in the matrix of the membrane (60% w/w) and a low thickness (50 μm), for a desirability value of 0.81 and the following predicted responses: $\tau_{t,Ni}$ = 7.285%; $\tau_{t,Co}$ = 5.460%; $\tau_{t,Cr}$ = 3.268%; $\tau_{t,Zn}$ = 8.690%; $\tau_{t,T}$ = 5.088%.

3.2.3. Modeling of the amount of metal ions fixed within the PIMs

Table 9 presents the percentages of Ni, Co, Cr and Zn fixed inside the PIMs after 6 h processing, calculated by Eqs. (5) and (6).

The results showed a maximum percentage of metal ions fixed within the membranes obtained in run 8 for all metal ions; this corresponds to the maximum of X_1 (initial concentration of metals), X_2 (the carrier ratio) and X_3 (the membrane thickness). This means that the three studied

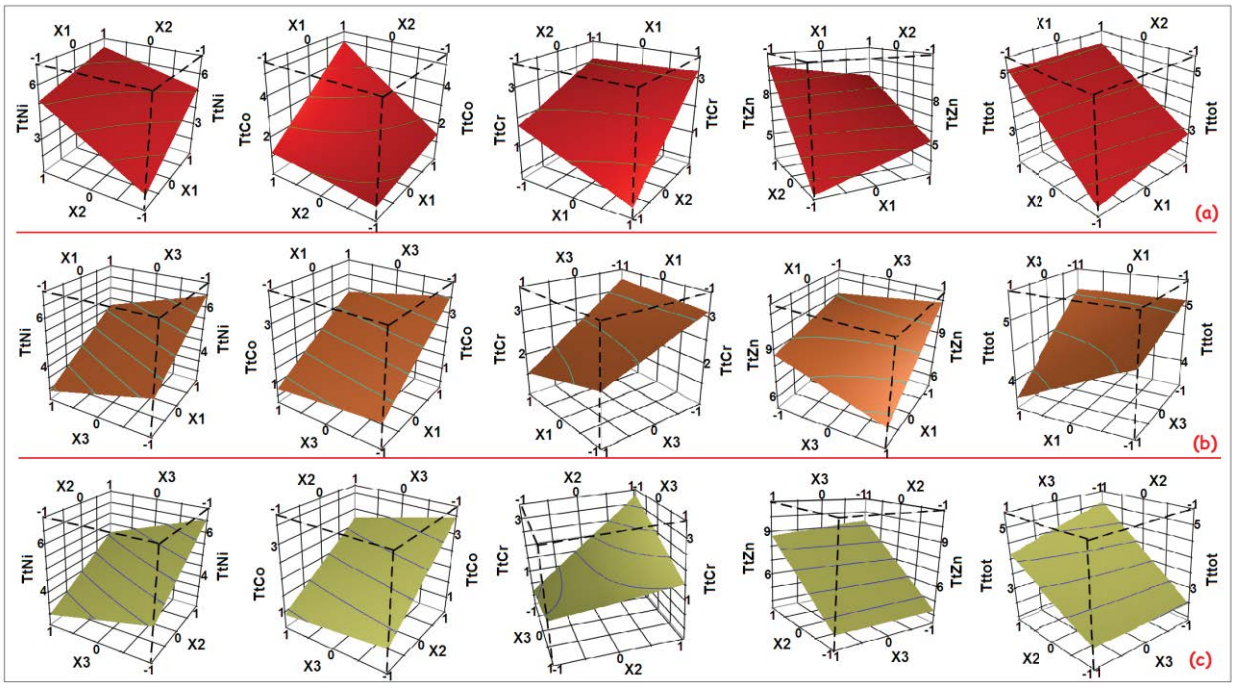

Fig. 6. 3D-plot of the response surfaces for the percentage of metals transferred vs.: (a) X_1 and X_2, (b) X_1 and X_3, and (c) X_2 and X_3.

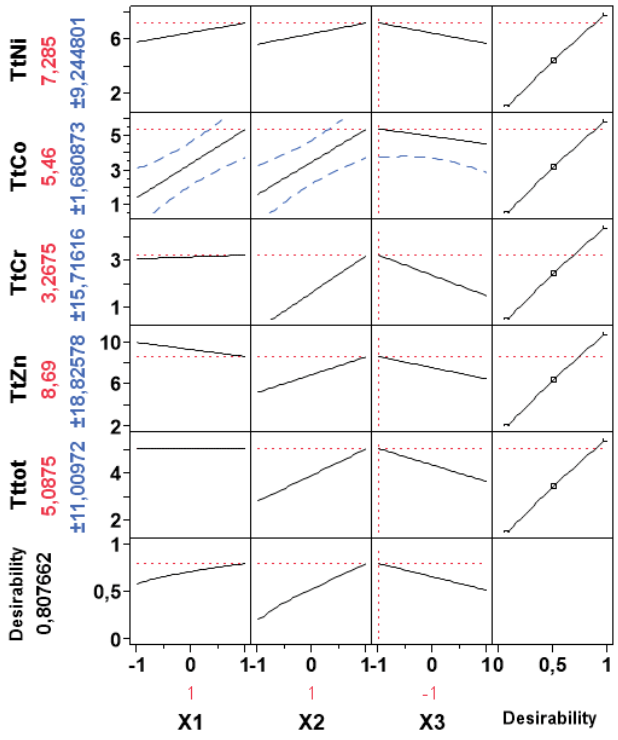

Fig. 7. Desirability function for the optimization of the percentage of metal ions transferred.

Table 9
Percentage of metals fixed inside the PIMs

Run (ref.)	Coded factors			Amount of metals retained (%)				
	X_1	X_2	X_3	Ni	Co	Cr	Zn	Total
Run 1	–	–	–	24.76	7.56	14.73	13.67	15.18
Run 2	+	–	–	28.50	8.50	15.76	14.12	16.72
Run 3	–	+	–	27.02	8.20	15.44	14.08	16.19
Run 4	+	+	–	29.98	9.13	16.70	15.64	17.86
Run 5	–	–	+	30.12	12.32	16.87	17.32	19.16
Run 6	+	–	+	33.57	16.01	17.43	21.45	22.12
Run 7	–	+	+	31.78	15.14	17.23	17.67	20.46
Run 8	+	+	+	37.43	17.43	21.93	25.13	25.48

parameters have a positive effect on the fixation of metallic ions inside the membrane, in different proportions depending on the metal. The corresponding maximum amounts found in run 8 were equal to 37.43, 17.43, 21.93 and 25.13% for Ni, Co, Cr and Zn, respectively, while the total percentage of metal ions fixed was equal to 25.48%. The results in Table 9 showed also that the fixation order of metal ions inside the synthesized PIMs is Ni > Zn > Cr > Co. The mean amount of Ni fixed inside the membranes was found to be equal to two and half times that of Co and more than one and half times those of Zn and Cr.

Table 10 gathers the results of the modelization of the percentage of metal ions fixed inside the PIMs and their statistical analysis (ANOVA). Based on *p*-values, except for Co for which X_3 is significant, the effects of linear and interaction terms are not significant for the other metal ions at a confidence level of 95%. For all metal ions, X_3 had the most significant effect followed by X_1 according to this order: $X_3 > X_1 > X_2 > X_1X_3 > X_2X_3 > X_1X_2$ for Ni; $X_3 > X_1 > X_2 > X_1X_3 > X_2X_3 > X_1X_2$ for Co; $X_3 > X_1 > X_2 > X_1X_2 > X_2X_3 > X_1X_3$ for Cr; $X_3 > X_1 > X_1X_3 > X_2 > X_1X_2 > X_2X_3$ for Zn; $X_3 > X_1 > X_2 > X_1X_3 > X_2X_3 > X_1X_2$ for all metals (total percentage of metal ions fixed). It should be noted that except the effect of the interaction X_1X_2, all of the other effects were positive suggesting that all parameters favor the fixation of metal ions inside the membranes. Moreover, the interaction X_1X_3, that is, between the initial concentration and the membrane thickness was statistically significant indicating an antagonistic effect between these variables on the studied response.

The models developed to fit experimental data for each response are described by Eqs. (19)–(23):

$$\tau_{f,\mathrm{Ni}} = 30.3950 + 1.9750x_1 + 1.1575x_2 + 2.8300x_3 + 0.1775x_1x_2 + 0.3000x_1x_3 + 0.2225x_2x_3 \quad (19)$$

$$\tau_{f,\mathrm{Co}} = 11.7863 + 0.9813x_1 + 0.6888x_2 + 3.4388x_3 - 0.1763x_1x_2 + 0.5138x_1x_3 + 0.3713x_2x_3 \quad (20)$$

$$\tau_{f,\mathrm{Cr}} = 17.0113 + 0.9438x_1 + 0.8138x_2 + 1.3538x_3 + 0.5463x_1x_2 + 0.3713x_1x_3 + 0.4013x_2x_3 \quad (21)$$

$$\tau_{f,\mathrm{Zn}} = 17.3850 + 1.7000x_1 + 0.7450x_2 + 3.0075x_3 + 0.5550x_1x_2 + 1.1975x_1x_3 + 0.2625x_2x_3 \quad (22)$$

$$\tau_{f,T} = 19.1463 + 1.3988x_1 + 0.8513x_2 + 2.6588x_3 + 0.2738x_1x_2 + 0.5963x_1x_3 + 0.3138x_2x_3 \quad (23)$$

The statistics used to test the adequacy of the models at confidence level of 95% are summarized in Table 10. The coefficient of determination (R^2) varied from 94.34% for Cr to 99.78% for Co, suggesting that the predicted models reasonably represent the observed values.

Fig. 8a–c depicts via 3D response surface plot, the percentage of fixed metal ions vs. two experimental factors while the third factor is kept constant at its central value (*cf.* Table 1). It can be seen from these figures that all linear and interaction effects were positive and that there is an important interaction between X_1 and X_2 and also between X_1 and X_3, especially for Cr and Zn. Indeed, the carrier ratio (X_2) favored the fixation of these metals inside the PIMs, but mainly when the initial concentration was at its high level (200 ppm), and in the same way, the initial concentration favored their fixation, but mainly when the carrier ratio was at its high level (60% w/w).

On the other hand, Fig. 8b shows that for average values in the range of studied ratio of the carrier (35% w/w), the effect of X_1 is maximal when X_3 is at high levels, and the effect of X_3 is maximal when X_1 is fixed at high levels, which indicates that the driving force due to the concentration gradient urges the metal ions into the membrane, but that the diffusion step inside the membrane is critical.

Table 10
Statistical analysis of results concerning the percentage of metals fixed inside the PIMs

Parameter	Ni			Co			Cr			Zn			Total		
	MC[a]: α_i	SE[b]	*p*-value	MC[a]: α_i	SE[b]	*p*-value	MC[a]: α_i	SE[b]	*p*-value	MC[a]: α_i	SE[b]	*p*-value	MC[a]: α_i	SE[b]	*p*-value
Constant	30.3950	0.373	0.008*	11.7863	0.174	0.009*	17.0113	0.489	0.018*	17.3850	0.278	0.010*	19.1463	0.241	0.008*
X_1	1.9750	0.373	0.119	0.9813	0.174	0.112	0.9438	0.489	0.304	1.7000	0.278	0.103	1.3988	0.241	0.109
X_2	1.1575	0.373	0.198	0.6888	0.174	0.157	0.8138	0.489	0.344	0.7450	0.278	0.227	0.8513	0.241	0.176
X_3	2.8300	0.373	0.083	3.4388	0.174	0.032*	1.3538	0.489	0.221	3.0075	0.278	0.059	2.6588	0.241	0.058
X_1X_2	0.1775	0.373	0.717	–0.1763	0.174	0.495	0.5463	0.489	0.465	0.5550	0.278	0.295	0.2738	0.241	0.460
X_1X_3	0.3000	0.373	0.568	0.5138	0.174	0.208	0.3713	0.489	0.586	1.1975	0.278	0.145	0.5963	0.241	0.245
X_2X_3	0.2225	0.373	0.657	0.3713	0.174	0.279	0.4013	0.489	0.562	0.2625	0.278	0.518	0.3138	0.241	0.417
R^2	0.9898			0.9978			0.9434			0.9946			0.9944		
Adj. R^2	0.9284			0.9846			0.6039			0.9625			0.9606		
R-SD[c]	1.0536			0.4914			1.3824			0.7849			0.6823		

[a]Model coefficients based on Eq. (8);
[b]Standard error;
[c]Residual standard deviation;
*Significant effect: $p < 0.05$.

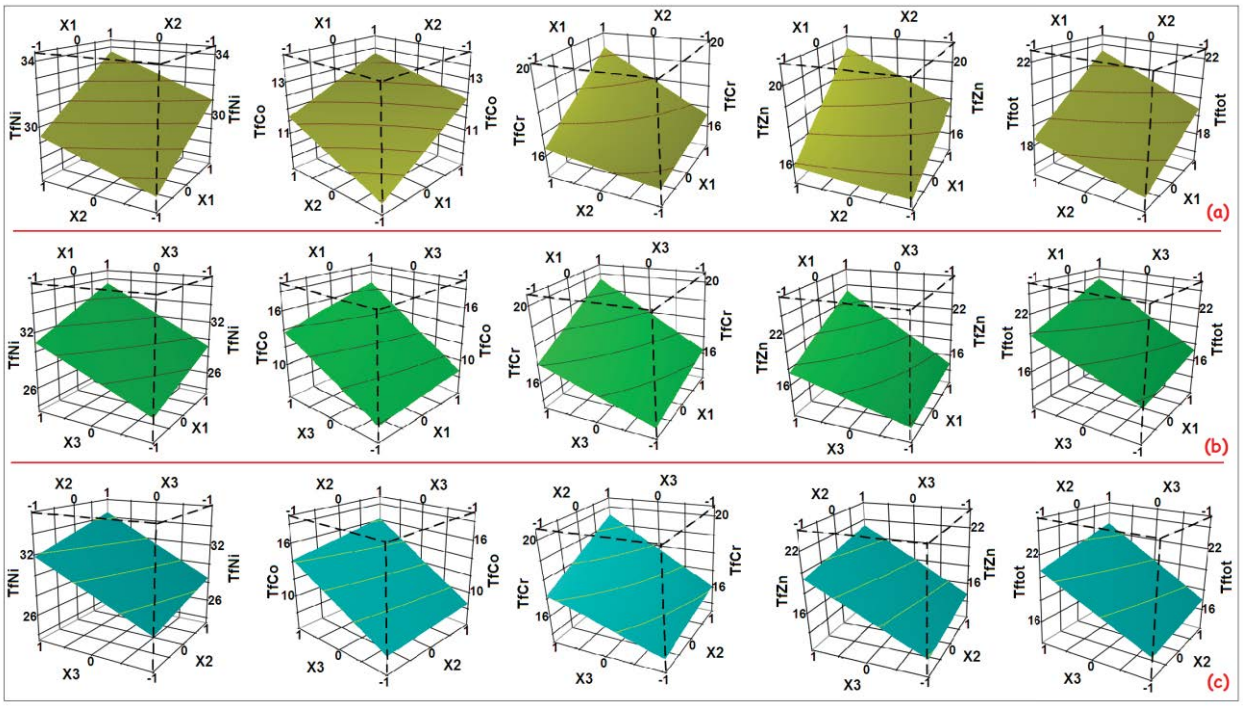

Fig. 8. 3D-plot of the response surfaces for the percentage of metals fixed vs.: (a) X_1 and X_2, (b) X_1 and X_3, and (c) X_2 and X_3.

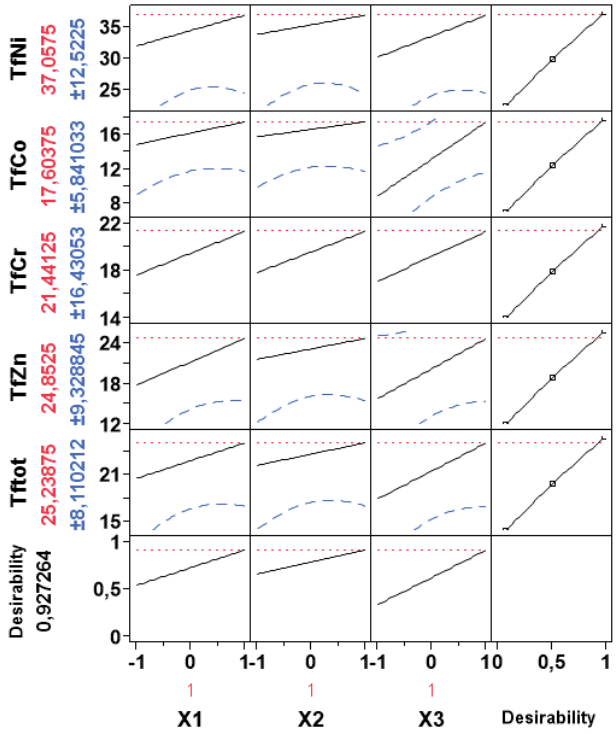

Fig. 9. Desirability function for the optimization of the percentage of metal ions fixed.

Thus, in the case of this response, the use of the desirability approach to optimize the process may be confusing, because the purpose is not to maximize or to minimize the amount of metals fixed inside the membrane, but to ensure that the metal ions cross as fast as possible the membrane thickness. To make that possible with our system (PEG/CTA), the solution would be to make changes on the chemical properties of both source and receiving solutions in order to achieve mass transport from the source to the receiving phase within a reasonable timeframe. Indeed, the actual transport phenomena in PIMs are quite complex and can be strongly influenced by both the physicochemical properties of the carrier and the target solute, but also by the chemical composition of the membrane as well as the source and receiving solutions [37–40].

Fig. 9 depicts the desirability function for the optimization of the process in order to have a maximum of each metal fixed within the membrane. The operating conditions that provide the "most desirable" response values, that is, a maximum percentage fixed, corresponds to a high initial concentration for each metal (200 ppm), a high ratio of the carrier in the matrix of the membrane (60% w/w) and a high thickness (65 μm), for a desirability value of 0.93 and the following predicted responses: $\tau_{f,Ni}$ = 37.058%; $\tau_{f,Co}$ = 17.604%; $\tau_{f,Cr}$ = 21.441%; $\tau_{f,Zn}$ = 24.852%; $\tau_{f,T}$ = 25.239%.

4. Conclusion

In the present study, a membrane process involving CTA-based PIMs and aiming the simultaneous removal of Ni^{2+}, Co^{2+}, Cr^{3+} and Zn^{2+} from aqueous solutions, is modeled and optimized using a 2^3 full factorial design. The effects of initial metal ion concentration (X_1), carrier content (X_2) and membrane thickness (X_3) were investigated on the matter fluxes crossing the PIMs (J), the amount of metal ions fixed inside the membrane (τ_f) and the amount of metal ions

transferred through the PIMs (τ_t) to a receiving compartment. The following conclusions were drawn from the study:

- The order of selectivity of the synthesized PIMs for metal ions is: $Zn^{2+} > Ni^{2+} > Cr^{3+} > Co^{2+}$.
- The order of significance of the factors' effects is: $X_1 > X_2 > X_3$.
- The analysis of variance (ANOVA) revealed that X_1 and X_2 have positive effect on J, τ_f and τ_t while X_3 has a negative effect on J and τ_t.
- The elaborated models for each studied response fit adequately the experimental data (determination coefficient: R^2 = 84.70%–99.99%; standard deviation: SD = 0.0021 – 1.58).
- The desirability-based optimization indicated that: J_{max} and τ_{tmax} are obtained for X_{1max} (200 ppm), X_{2max} (60% w/w) and X_{3min} (50 μm), for a desirability value of 0.93 and 0.81, respectively, while τ_{fmax} is obtained for X_{1max}, X_{2max} and X_{3max} (65 μm), for a desirability value of 0.93.

Acknowledgments

The authors gratefully acknowledge the financial support received from "Région Nouvelle Aquitaine" through n°14/RPC-R-052 agreement.

References

[1] Y. Lu, W. Liu, J. Liu, X. Li, S. Zhang, A review on 2D porous organic polymers for membrane-based separations: processing and engineering of transport channels, Adv. Membr., 1 (2021) 100014, doi: 10.1016/j.advmem.2021.100014.
[2] C. Charcosset, Membrane processes in biotechnology: an overview, Biotechnol. Adv., 24 (2006) 482–492.
[3] H.I. Turgut, V. Eyupoglu, R.A. Kumbasar, I. Sisman, Alkyl chain length dependent Cr(VI) transport by polymer inclusion membrane using room temperature ionic liquids as carrier and PVDF-co-HFP as polymer matrix, Sep. Purif. Technol., 175 (2017) 406–417.
[4] E.R. de San Miguel, M. Monroy-Barreto, J.C. Aguilar, A.L. Ocampo, J. de Gyves, Structural effects on metal ion migration across polymer inclusion membranes: dependence of membrane properties and transport profiles on the weight and volume fractions of the components, J. Membr. Sci., 379 (2011) 416–425.
[5] L.D. Nghiem, P. Mornane, I.D. Potter, J.M. Perera, R.W. Cattrall, S.D. Kolev, Extraction and transport of metal ions and small organic compounds using polymer inclusion membranes (PIMs), J. Membr. Sci., 281 (2006) 7–41.
[6] X.-j. Qiu, J. Tang, J. Tan, H.-p. Hu, X.-b. Ji, J.-g. Hu, Selective recovery of Cu(II) through polymer inclusion membranes mediated with 2-aminomethylpyridine derivatives, Trans. Nonferrous Met. Soc. China, 31 (2021) 3591–3601.
[7] J. García-Beleño, E. Rodríguez de San Miguel, Optimization of Cr(III) transport in a polymer inclusion membrane system through experimental design strategies, Chem. Pap., 76 (2022) 2235–2247.
[8] M.I.G. Almeida, R.W. Cattrall, S.D. Kolev, Recent trends in extraction and transport of metal ions using polymer inclusion membranes (PIMs), J. Membr. Sci., 415 (2012) 9–23.
[9] A.J. Schow, R.T. Peterson, J.D. Lamb, Polymer inclusion membranes containing macrocyclic carriers for use in cation separations, J. Membr. Sci., 111 (1996) 291–295.
[10] D. Wang, J. Hu, Y. Li, M. Fu, D. Liu, Q. Chen, Evidence on the 2-nitrophenyl octyl ether (NPOE) facilitating copper(II) transport through polymer inclusion membranes, J. Membr. Sci., 501 (2016) 228–235.
[11] B. Wang, F. Liu, F. Zhang, M. Tan, H. Jiang, Y. Liu, Y. Zhang, Efficient separation and recovery of cobalt(II) and lithium(I) from spent lithium-ion batteries (LIBs) by polymer inclusion membrane electrodialysis (PIMED), Chem. Eng. J., 430 (2022) 132924, doi: 10.1016/j.cej.2021.132924.
[12] A.H. Blitz-Raith, R. Paimin, R.W. Cattrall, S.D. Kolev, Separation of cobalt(II) from nickel(II) by solid-phase extraction into Aliquat 336 chloride immobilized in poly(vinyl chloride), Talanta, 71 (2007) 419–423.
[13] S. Kagaya, R.W. Cattrall, S.D. Kolev, Solid-phase extraction of cobalt(II) from lithium chloride solutions using a poly(vinyl chloride)-based polymer inclusion membrane with Aliquat 336 as the carrier, Anal. Sci., 27 (2011) 653–657.
[14] E. Radzyminska-Lenarcik, I. Pyszka, W. Urbaniak, New polymer inclusion membranes in the separation of palladium, zinc and nickel ions from aqueous solutions, Polymers, 13 (2021) 1424, doi: 10.3390/polym13091424.
[15] B. Pośpiech, W. Walkowiak, Separation of copper(II), cobalt(II) and nickel(II) from chloride solutions by polymer inclusion membranes, Sep. Purif. Technol., 57 (2007) 461–465.
[16] B. Hoque, M.I.G. Almeida, R.W. Cattrall, T.G. Gopakumar, S.D. Kolev, Effect of cross-linking on the performance of polymer inclusion membranes (PIMs) for the extraction, transport and separation of Zn(II), J. Membr. Sci., 589 (2019) 117256, doi: 10.1016/j.memsci.2019.117256.
[17] S.D. Kolev, Y. Baba, R.W. Cattrall, T. Tasaki, N. Pereira, J.M. Perera, G.W. Stevens, Solid phase extraction of zinc(II) using a PVC-based polymer inclusion membrane with di(2-ethylhexyl) phosphoric acid (D2EHPA) as the carrier, Talanta, 78 (2009) 795–799.
[18] J. Kozlowska, C.A. Kozłowski, J.J. Koziol, Transport of Zn(II), Cd(II), and Pb(II) across CTA plasticized membranes containing organophosphorous acids as an ion carriers, Sep. Purif. Technol., 57 (2007) 430–434.
[19] L.L. Zhang, R.W. Cattrall, S.D. Kolev, The use of a polymer inclusion membrane in flow injection analysis for the on-line separation and determination of zinc, Talanta, 84 (2011) 1278–1283.
[20] C.V. Gherasim, G. Bourceanu, R.I. Olariu, C. Arsene, A novel polymer inclusion membrane applied in chromium(VI) separation from aqueous solutions, J. Hazard. Mater., 197 (2011) 244–253.
[21] O. Kebiche-Senhadji, S. Tingry, P. Seta, M. Benamor, Selective extraction of Cr(VI) over metallic species by polymer inclusion membrane (PIM) using anion (Aliquat 336) as carrier, Desalination, 258 (2010) 59–65.
[22] G. Salazar-Alvarez, A.N. Bautista-Flores, E.R. de San Miguel, M. Muhammed, J. de Gyves, Transport characterisation of a PIM system used for the extraction of Pb(II) using D2EHPA as carrier, J. Membr. Sci., 250 (2005) 247–257.
[23] S.P. Kusumocahyo, T. Kanamori, K. Sumaru, S. Aomatsu, H. Matsuyama, M. Teramoto, T. Shinbo, Development of polymer inclusion membranes based on cellulose triacetate: carrier-mediated transport of cerium(III), J. Membr. Sci., 244 (2004) 251–257.
[24] A. Garcia-Rodríguez, V. Matamoros, S.D. Kolev, C. Fontàs, Development of a polymer inclusion membrane (PIM) for the preconcentration of antibiotics in environmental water samples, J. Membr. Sci., 492 (2015) 32–39.
[25] S.M.S. Shahabadi, A. Reyhani, Optimization of operating conditions in ultrafiltration process for produced water treatment via the full factorial design methodology, Sep. Purif. Technol., 132 (2014) 50–61.
[26] D.C. Montgomery, Design and Analysis of Experiments, John Wiley & Sons, Hoboken, 2017.
[27] A. Cherfi, K. Dehak-Oughlissi, S.A. Bali, T.B. Meddour, Technical-economic study of PVC-based formulations intended to industrial 3-wire electric cables, using a full factorial design methodology, J. Elastomers Plast., 55 (2023) 426–454.
[28] C. Charcosset, A. Cherfi, J.C. Bernengo, Characterization of microporous membrane morphology using confocal scanning laser microscopy, Chem. Eng. Sci., 55 (2000) 5351–5358.

[29] N.R. Costa, J. Lourenço, Z.L. Pereira, Desirability function approach: a review and performance evaluation in adverse conditions, Chemom. Intell. Lab. Syst., 107 (2011) 234–244.
[30] G. Derringer, R. Suich, Simultaneous optimization of several response variables, J. Qual. Technol., 12 (1980) 214–219.
[31] E. Radzyminska-Lenarcik, I. Pyszka, M. Ulewicz, Separation of Zn(II), Cr(III), and Ni(II) ions using the polymer inclusion membranes containing acetylacetone derivative as the carrier, Membranes, 10 (2020) 88, doi: 10.3390/membranes10050088.
[32] P. Szczepański, H. Guo, K. Dzieszkowski, Z. Rafiński, A. Wolan, K. Fatyeyeva, W. Kujawski, New reactive ionic liquids as carriers in polymer inclusion membranes for transport and separation of Cd(II), Cu(II), Pb(II), and Zn(II) ions from chloride aqueous solutions, J. Membr. Sci., 638 (2021) 119674, doi: 10.1016/j.memsci.2021.119674.
[33] J. Konczyk, W. Ciesielski, Calixresorcin[4]arene-mediated transport of Pb(II) ions through polymer inclusion membrane, Membranes, 11 (2021) 285, doi: 10.3390/membranes11040285.
[34] B. Gajda, R. Plackowski, A. Skrzypczak, M.B. Bogacki, Facilitated transport of copper(II) across polymer inclusion membrane with triazole derivatives as carrier, Membranes, 10 (2020) 201, doi: 10.3390/membranes10090201.
[35] C. Zhang, Y. Mu, S. Zhao, W. Zhang, Y. Wang, Lithium extraction from synthetic brine with high Mg^{2+}/Li^{+} ratio using the polymer inclusion membrane, Desalination, 496 (2020) 114710, doi: 10.1016/j.desal.2020.114710.
[36] H. Kazemzadeh, J. Karimi-Sabet, J. Towfighi Darian, A. Adhami, Evaluation of polymer inclusion membrane efficiency in selective separation of lithium ion from aqueous solution, Sep. Purif. Technol., 251 (2020) 117298, doi: 10.1016/j.seppur.2020.117298.
[37] J.C. Aguilar, E.R. de San Miguel, J. de Gyves, R.A. Bartsch, M. Kim, Design, synthesis and evaluation of diazadibenzo-crown ethers as Pb^{2+} extractants and carriers in plasticized cellulose triacetate membranes, Talanta, 54 (2001) 1195–1204.
[38] C. Kozłowski, W. Apostoluk, W. Walkowiak, A. Kita, Removal of Cr(VI), Zn(II) and Cd(II) ions by transport across polymer inclusion membranes with basic ion carriers, Physicochem. Probl. Miner. Process., 36 (2002) 115–122.
[39] A.Y. Nazarenko, J.D. Lamb, Selective transport of lead(II) and strontium(II) through a crown ether-based polymer inclusion membrane containing dialkylnaphthalenesulfonic acid, J. Inclusion Phenom. Mol. Recognit. Chem., 29 (1997) 247–258.
[40] W. Walkowiak, R.A. Bartsch, C. Kozlowski, J. Gega, W.A. Charewicz, B. Amiri-Eliasi, Separation and removal of metal ionic species by polymer inclusion membranes, J. Radioanal. Nucl. Chem., 246 (2000) 643–650.